

Magnetic-force microscopy of vortices in thin niobium films: Correlation between the vortex distribution and the thickness-dependent film morphology

A. VOLODIN¹, K. TEMST¹, C. VAN HAESENDONCK¹, Y. BRUYNSERAEDE¹,
M. I. MONTERO² and I. K. SCHULLER²

¹ *Laboratorium voor Vaste-Stoffysica en Magnetisme, Katholieke Universiteit Leuven
Celestijnenlaan 200 D, B-3001 Leuven, Belgium*

² *Department of Physics, University of California-San Diego
La Jolla, CA 92093-0319, USA*

(received 5 June 2001; accepted in final form 15 February 2002)

PACS. 74.60.Ge – Flux pinning, flux creep, and flux-line lattice dynamics.

PACS. 68.37.Rt – Magnetic force microscopy (MFM).

PACS. 74.76.Db – Conventional superconducting films.

Abstract. – We demonstrate the possibility to reliably image vortices in superconducting Nb films with a low-temperature magnetic-force microscope. Our force microscope enables to monitor the surface topography as well, allowing to correlate the location of the vortices with specific topographic features. For Nb films of different thickness (32 nm–87 nm) and different T_c (7.9 K–9.1 K) we studied how the vortex configuration changes when changing the applied magnetic field under field-cooled conditions (1 mT–5 mT). We find that the vortex pinning preferentially occurs in between the grains appearing at the film surface. This is consistent with a distribution of pinning centers which is governed by the columnar growth of the Nb films. For thicker Nb films the vortex arrangement is no longer dominated by pinning alone, and there appear short-range correlations in the vortex lattice. The short-range correlations are enhanced when increasing the applied magnetic field.

Introduction. – With the advent of high-temperature superconductivity, the interest in obtaining materials which are able to carry very high superconducting current densities in the presence of a magnetic field has revived. In particular, the direct interplay between the critical current density and the specific defect structures has attracted a lot of attention [1]. During the last few years there also emerged a strong interest to understand the flux pinning properties of artificial defects introduced by microfabrication (holes) [2] or by ion irradiation (tracks) [3]. The experiments indicate a dramatic increase of the pinning when there is a matching between the flux line lattice and the underlying array of pinning centers. The matching effects are less pronounced for thin Nb films which tend to contain a rather high density of intrinsic, randomly distributed defects. Nevertheless, when the Nb film is covering an array of magnetic dots, the flux pinning process is considerably affected [4].

With the development of scanning probe microscopy, exciting new tools have become available to directly visualize the distribution of the magnetic vortices and to link this distribution to the presence of specific nanometer-scale defects. While most of the experiments focussed on scanning tunnelling microscopy, the magnetic force microscope (MFM) has been used to investigate the vortex arrangement only in a few cases [5, 6]. Here, we show that the MFM allows to visualize the changes in the vortex distribution which occur in thin Nb films when changing the film thickness and the applied magnetic field. Our low-temperature MFM is able to detect the magnetic stray field of the vortices and the sample topography at the same sample location. This way, we are able to establish a direct correlation between the position of the vortices and the presence of topographical features related to the film grain boundaries.

Experiment. – The Nb thin films have been deposited by electron beam evaporation in an ultra high vacuum molecular-beam epitaxy (MBE) system with a base pressure around 10^{-10} mbar. The deposition of the thin films onto oxidized Si (100) wafers is performed at room temperature at a rate of about 0.01 nm/s [7]. The film thickness is determined by low-angle X-ray scattering. The high-angle diffraction spectra confirm that the Nb thin films are polycrystalline with a preferred growth along the (110) direction, but with a random distribution of the in-plane grain orientation. Electrical transport measurements reveal an increase of the transition temperature T_c from 7.5 K towards the bulk value 9.2 K when increasing the Nb film thickness t from 25 nm to 100 nm. Both the transition width (≤ 0.1 K) and the normal-state resistivity at 10 K (10–15 $\mu\Omega\text{cm}$) confirm the quality of our MBE grown Nb films.

Our low-temperature MFM is based on cantilevers integrated with piezoresistive displacement detection [8, 9]. The sensing element is a piezoresistor embedded in the arms of the cantilever. The resistance change of the piezoresistor by stresses due to cantilever deflection can easily be measured. The piezoresistive cantilevers are commercially available (Park Scientific Instruments). The fundamental resonance frequency is in the range 30–50 kHz, while the force constant is about 1 N/m. Such cantilevers are ideally suited for operation at low temperatures, because they do not require optical detection of the cantilever deflection with a complicated *in situ* adjustment of the optical beam. The cantilevers incorporate sharpened Si tips at the end. In order to considerably enhance the sensitivity of the piezoresistive dynamic detection, we rely on the operation of the cantilevers at a higher flexural mode [10]. The cantilevers are electrically connected to a cryogenic resistance-to-voltage conversion circuit [11]. The major advantages of oscillating the cantilevers at higher frequencies (0.6–1 MHz) are i) an increase of the ultimate sensitivity to force gradients (0.2 pN/nm), and ii) a noticeable decrease of the electrical-noise level. This allows to minimize the heat dissipation for a given signal-to-noise ratio and to minimize the magnetic charge on the tip in order to decrease the influence of the MFM tip fringe field on weakly pinned vortices. MBE deposition is used to grow on top of the Si tips two 25 nm thick Co layers separated by a 2 nm thick Au layer. Oblique incidence deposition minimizes the coated area by restricting the magnetic-film growth to one side of the tip. This optimized Co/Au multilayer coating of the tip as well as the relatively large tip-sample separation (20–50 nm) turns out to considerably decrease the stray field from the tip acting on the sample surface.

All measurements reported in this paper have been performed under field-cooled conditions. Our MFM is able to resolve individual vortices in the Nb films when cooling the films below T_c in relatively low magnetic fields (< 10 mT) [9]. This is confirmed by the fact that the density of vortices observed with our MFM corresponds to the ratio between the applied magnetic field and the superconducting flux quantum $\Phi_0 = h/2e = 2.07 \times 10^{-15}$ Wb = 2.07 mT/ μm^2 . An increase of the field above 10 mT leads to an almost complete loss of the MFM contrast due to the overlap between the magnetic fields of neighbouring vortices.

In order to image the vortices, the following procedure has been used. The tip is first brought into contact with the sample surface at an elevated temperature around 10 K, *i.e.*, above T_c in the normal state. Scanning in the x and y directions allows to determine the angle between the plane of the sample surface and the plane of the scanner. The (x, y) scan plane is then adjusted to coincide with the investigated Nb surface. Next, the tip is raised above the surface towards a height exceeding 1 nm. After cooling down to 4.3 K in a magnetic field parallel to the z -direction (perpendicular to the film surface), the tip-sample separation is decreased to a fixed separation, ranging between 20 and 50 nm. Finally, while scanning the tip across the (x, y) -plane, we record the phase shift of the oscillation of the cantilever due to the magnetic interaction between the sample and the tip. This procedure provides the magnetic-force image and allows to avoid the disturbance of the superconducting vortex lattice by a very short distance between the magnetic tip and the sample surface.

The stray field produced by the tip may have an influence on the superconducting Nb sample. Measurements taken at zero external magnetic field point towards the existence of an offset field $B_{\text{tip}} = 0.3\text{--}0.5\text{ mT}$, which corresponds to the extra field induced by our MFM tips [12]. The field B_{tip} is sufficiently small to be able to perform reliable non-invasive imaging of the magnetic vortices distribution. Previous experiments with our low-temperature MFM demonstrated the possibility to image the regular Abrikosov vortex lattice in crystals of NbSe₂ [9].

In order to measure the Nb surface topography the tip-to-sample distance is decreased to allow operation of the MFM in the near-field non-contact atomic-force microscopy (AFM) regime, providing a pure topographic contrast with our microscope. The topographic image is acquired at the same position as the magnetic image. Below, we will describe in detail how we are able to correlate with a very high spatial resolution the location of the vortices with specific topographic features of the Nb film surfaces.

Experimental results. – Figure 1(a) shows a typical example of an unfiltered MFM image of the vortex distribution taken at 4.3 K under field-cooled conditions at 4 mT for the thin-film sample Nb2 (see table I). The corresponding topographic AFM image at the same location is shown in fig. 1(b). The surface appears textured with ellipsoidal grains typical of thin Nb films [13]. In order to determine the exact location of the vortices with respect to features appearing in the topographic AFM image, it is necessary to take into account the asymmetric distribution of the magnetic charge present on the tip [14]. The asymmetry shifts the magnetic image with respect to the topographic image. In order to determine this shift, Hug *et al.* [14] suggested to rely on a transfer function approach. The transfer function of the tip can be inferred from the geometrical shape of the tip [15]. We used an alternative approach which is based on measurements of a microfabricated gold ring [16]. The MFM image and the topographic image are recorded while sending a current of several mA through the ring. We analyzed MFM images of rings with diameters of 1 μm and 5 μm and a width of 0.2 μm obtained at different heights (10–60 nm). The shift of the MFM image is calculated

TABLE I – *Relevant parameters of the thin Nb films which have been studied in detail.*

| Sample | Nb1 | Nb2 | Nb3 |
|--------------------------|-----|-----|-----|
| Thickness (nm) | 32 | 33 | 87 |
| RMS roughness (nm) | 1.4 | 1.4 | 2 |
| Grain size (nm) | 24 | 27 | 32 |
| Critical temperature (K) | 7.9 | 8.4 | 9.1 |

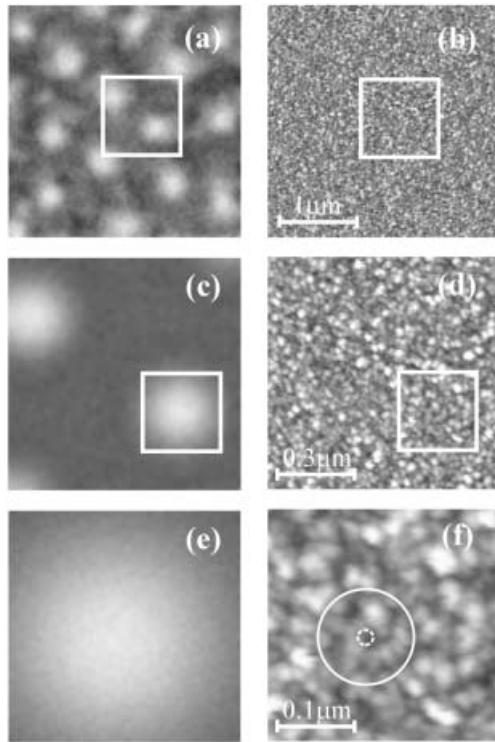


Fig. 1

Fig. 1 – (a) Raw data MFM image ($3 \times 3 \mu\text{m}^2$) for the Nb film Nb2 (see table I) which was cooled in an external field of 4 mT. (b) Surface topography acquired at the same location (the grey scale contrast corresponds to 8 nm). (c) Enlarged MFM image ($1 \times 1 \mu\text{m}^2$, see white squares in (a), (b)) after applying a low-pass filter and (d) the corresponding topographic image. The white squares in (c), (d) indicate the location of the enlarged images shown in (e) and in (f). The white circle in (f) corresponds to the distance at which the stray field emanating from the vortex has decreased to $1/e$ of its maximum value. The dotted circle defines an area with diameter $2\xi \approx 22 \text{ nm}$ [7] (ξ is the superconducting coherence length).

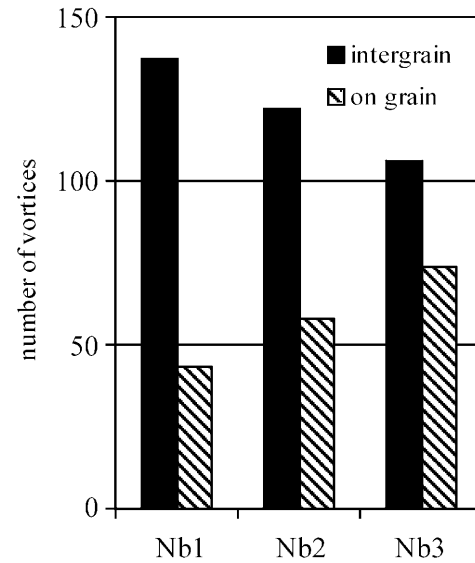


Fig. 2

Fig. 2 – Histogram illustrating the preferential location of the vortices in between the grains of the Nb films with different thickness, *i.e.*, with different critical temperature T_c (see table I).

by comparing the coordinates of the geometrical center of the MFM image and the center of the topographic image, respectively. Calculated values of the shift for different tips (magnetic coating deposited during different MBE runs) range between 10 and 40 nm. The location of the vortices on the MFM images is determined by fitting a Gaussian profile to their MFM signal after filtering with a low-pass filter (see fig. 1(c), (e)). Taking into account the calculated shift of the MFM image with respect to the topographic image, we are able to infer the exact location of the magnetic vortices with respect to the surface topography shown in figs. 1(d) and (f). The accuracy of this procedure is estimated to be better than 10 nm, indicating that we are able to distinguish between on-grain and inter-grain flux pinning. The typical grain size of our films is 30 nm (see table I). We note that for our Nb films the diameter of the normal core of a vortex $2\xi \approx 22 \text{ nm}$ [7] (ξ is the superconducting coherence length) is smaller than the typical grain size.

Combining for each Nb film listed in table I the results of 9 different MFM measurements in an external field of 4 mT with the corresponding topographic images, we find that a larger fraction of the vortex pinning occurs in between the grains. This is illustrated by the histogram shown in fig. 2. The histograms further indicate that in thinner Nb films the preferential pinning at locations in between grains becomes more pronounced. This is consistent with a columnar growth of the Nb films. Obviously, the pinning mechanism for the Nb films cannot be explained by the presence of atomic-scale defects in between grains, because of the large value of the coherence length when compared to the size of such defects. On the other hand, the coherence length of about 11 nm for the Nb films is comparable to the size of the depressions in between the grains, and the protruding grains seem to be well coupled electrically. We therefore assume that pinning in between the protruding Nb grains occurs because of the considerable local reduction of the Nb film thickness. From the topographical image (fig. 1(f)) we infer a thickness reduction of 4 nm–8 nm or more than 1/8 of the film thickness, which should be sufficient to induce pinning in between grains. In the thicker Nb films with a higher T_c less vortices are pinned in between grains. This confirms that the

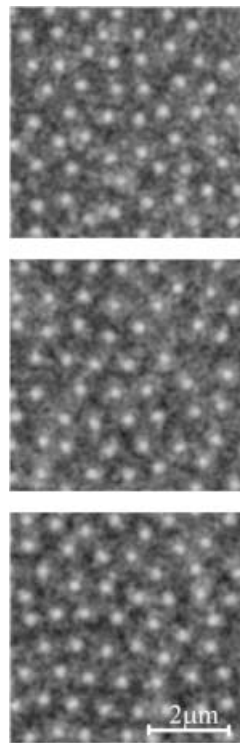


Fig. 3

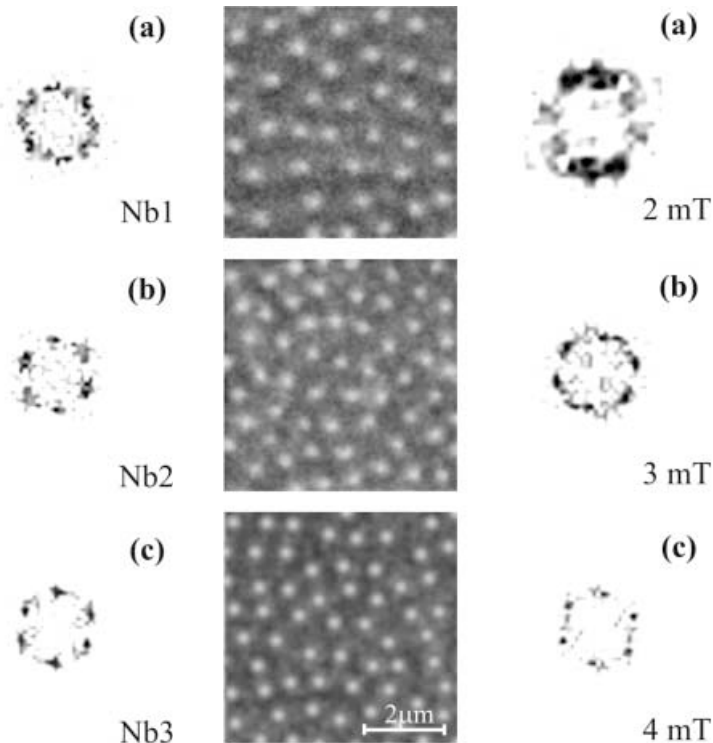


Fig. 4

Fig. 3 – Filtered MFM images ($6 \times 6 \mu\text{m}^2$) of the vortex arrangement and the corresponding two-dimensional Fourier transforms for Nb films with different thickness: (a) 32 nm, (b) 33 nm and (c) 87 nm (see table I). The films have been cooled in the presence of a magnetic field of 4 mT.

Fig. 4 – Filtered MFM images ($6 \times 6 \mu\text{m}^2$) of the vortex arrangement and the corresponding two-dimensional Fourier transforms for the Nb film with a thickness of 87 nm (see table I) for different applied magnetic fields: (a) 2 mT, (b) 3 mT, and (c) 4 mT.

vortex-vortex interaction becomes more dominant when compared to the pinning process in the thinner films. The tendency to form a more regular vortex lattice in the thicker films is illustrated in more detail in fig. 3, where we show the measured distribution of the vortices for 3 different film thicknesses together with the corresponding two-dimensional Fourier transform of the MFM images. As the film thickness is increased, the Fourier transform clearly reveals discrete spots.

A gradual ordering of the vortex lattice is also observed when increasing the applied magnetic field. This is illustrated in fig. 4, where the evolution of both the MFM image and the corresponding two-dimensional Fourier transform are shown for the Nb film Nb3 with $t = 87$ nm. The Fourier transforms in figs. 3 and 4 clearly reveal the emergence of an hexagonal Abrikosov vortex lattice when increasing the film thickness or the applied magnetic field. The appearance of the hexagonal lattice implies that the arrangement of vortices is no longer dominated by pinning alone, but also by the vortex-vortex interaction which induces the formation of short-range order in the vortex arrangement.

Conclusions. – We have demonstrated the possibility to reliably measure the magnetic stray field of vortices in superconducting Nb films with a low-temperature magnetic-force microscope, and to monitor the surface topography at the same location. This allows to correlate the location of the vortices with specific topographic features. We find that in our thin Nb films the vortex pinning preferentially occurs in between the grains composing the films. The preferential pinning becomes more pronounced in thinner Nb films. For Nb films of different thickness and different T_c we have studied in detail how the vortex configuration becomes more ordered when changing the applied magnetic field.

Finally, it should be mentioned that the sensitivity needed to image vortices with our force microscope is close to the thermodynamic noise limit [17] for the commercially available cantilevers. Presently, it is only possible to image vortices in relatively flat films. Consequently, further improvements of the piezoresistive detection are required to visualize the vortex arrangement in superconducting films with artificial arrays of well-characterized pinning centers [2, 4].

* * *

The work has been supported by the Fund for Scientific Research - Flanders (FWO), the Flemish Concerted Action (GOA) and the Belgian Inter-University Attraction Poles (IUAP) research programs, and by the US Department of Energy (US-DOE).

REFERENCES

- [1] DAM B., HUIJBREGTSE J. M., KLAASSEN F. C., VAN DER GEEST R. C. F., DOORNBOS G., RECTOR J. H., TESTA A. M., FREISEM S., MARTINEZ J. C., STÄUBLE-PÜMPIN B. and GRIESSEN R., *Nature*, **399** (1999) 439.
- [2] BAERT M., METLUSHKO V. V., JONCKHEERE R., MOSHCHALOV V. V. and BRUYNSEAEDE Y., *Phys. Rev. Lett.*, **74** (1995) 3269.
- [3] BEHLER S., PAN S. H., BERNASCONI M., JESS P., HUG H. J., FRITZ O. and GÜNTHERODT H.-J., *Phys. Rev. Lett.*, **72** (1994) 1750.
- [4] JACCARD Y., MARTIN J. I., CYRILLE M.-C., VELEZ M., VICENT J. L. and SCHULLER I. K., *Phys. Rev. B*, **58** (1998) 8232.
- [5] MOSER A., HUG H. J., PARASHIKOV I., STIEFEL B., FRITZ O., THOMAS H., BARATOFF A. and GÜNTHERODT H.-J., *Phys. Rev. Lett.*, **74** (1995) 1847.

- [6] MOSER A., HUG H. J., STIEFEL B. and GÜNTHERODT H.-J., *J. Magn. & Magn. Mater.*, **190-192** (1998) 114.
- [7] HOFFMANN A., Doctoral Thesis, University of California, San Diego (1999).
- [8] YUAN C. W., BATALLA E., ZACHER M., DE LOZANNE A. L., KIRK M. D. and TORTONESE M., *Appl. Phys. Lett.*, **65** (1994) 1308.
- [9] VOLODIN A., TEMST K., VAN HAESENDONCK C. and BRUYNSERAEDE Y., *Appl. Phys. Lett.*, **73** (1998) 1134.
- [10] VOLODIN A. and VAN HAESENDONCK C., *Appl. Phys. A*, **66** (1998) S305.
- [11] VOLODIN A., TEMST K., VAN HAESENDONCK C. and BRUYNSERAEDE Y., *Rev. Sci. Instrum.*, **71** (2000) 4468.
- [12] VOLODIN A., TEMST K., VAN HAESENDONCK C. and BRUYNSERAEDE Y., *Physica C*, **332** (2000) 156.
- [13] TARUTANI Y., HIRANO M. and KAWABE U., *Proc. IEEE*, **27** (1989) 1164.
- [14] HUG H. J., STIEFEL B., VAN SCHENDEL P. J. A., MOSER A., HOFER R., MARTIN S. and GÜNTHERODT H.-J., *J. Appl. Phys.*, **83** (1998) 5609.
- [15] VAN SCHENDEL P. J. A. *et al.*, *J. Appl. Phys.*, **88** (2000) 435.
- [16] KONG LINSHU and CHOU S. Y., *Appl. Phys. Lett.*, **70** (1997) 2043.
- [17] HUG H. J., STIEFEL B., VAN SCHENDEL P. J. A., MOSER A., MARTIN S. and GÜNTHERODT H.-J., *Rev. Sci. Instrum.*, **70** (1999) 3625.